minerals

MDPI

Article

Metamorphic Evolution of Garnet-Bearing Ultramafic Rocks in the Hujialin Area, Sulu Ultrahigh-Pressure Orogenic Belt, Eastern China

Zeli Wang [1], Shukai Zhang [1], Xu-Ping Li [1,*], Songjie Wang [1], Dan Wang [1], Fan-Mei Kong [1], Jianguo Liu [2], Zengsheng Li [3], Dapeng Li [3], Jian Wang [4] and Yongqiang Yang [5]

1 Shandong Key Laboratory of Depositional Mineralization and Sedimentary Minerals, Shandong University of Science and Technology, Qingdao 266590, China; Wangzl2458@sina.com (Z.W.); Zhangshukai1026@163.com (S.Z.); cugsongjie@foxmail.com (S.W.); wd601081125@163.com (D.W.); kongfanmei56@sdust.edu.cn (F.-M.K.)
2 College of Mining Engineering, North China University of Science and Technology, Tangshan 063210, China; liujg@ncst.edu.cn
3 Shandong Institute of Geological Sciences, Jinan 250013, China; lizengsheng@126.com (Z.L.); dpengli@126.com (D.L.)
4 College of Earth Sciences, Jilin University, Changchun 130061, China; Wangjian304@jlu.edu.cn
5 State Key Laboratory of Geological Processes, China University of Geosciences, Beijing 100083, China; yangyonq@cugb.edu.cn
* Correspondence: lixuping@sdust.edu.cn; Tel.: +86-8068-1139

Received: 26 January 2020; Accepted: 26 February 2020; Published: 29 February 2020

Abstract: The Rizhao Hujialin area is located in the central Sulu ultrahigh-pressure orogenic belt, where garnet clinopyroxenite is exposed in the upper part of an ultramafic rock complex and serpentinized dunite is exposed in its lower part. Based on textural criteria, the garnet clinopyroxenites were divided into three types: Equigranular garnet, porphyroclastic garnet, and megacrystic garnet pyroxenites. The garnet clinopyroxenites have convex-upward chondrite-normalized rare earth element patterns, large positive Pb anomalies, and depletion of high-field-strength elements (e.g., Nb, Zr, and Ti), suggesting a mantle source protolith overprinted by fluid metasomatism. Petrographic, mineral chemistry, phase equilibrium modeling, and zircon U–Pb geochronology data show that the evolutionary stages of the Hujialin garnet clinopyroxenites were as follows: Stage I: formation of the magmatic protoliths; stage II: formation of megacrystic garnet pyroxenite accompanying subduction; stage III: formation of porphyroclastic or equigranular garnet clinopyroxenite with a mineral assemblage of garnet + clinopyroxene + ilmenite + humite accompanying initial exhumation at ~215.0 ± 5.7 Ma; stage IV = progressive cooling and decompression associated with the crystallization of water-bearing minerals such as clinochlore and pargasite at 206 Ma; and Stage V = late epidote amphibolite-facies retrograde metamorphism producing a mineral assemblage of garnet + clinopyroxene + amphibole + chlorite + epidote + ilmenite at ~180–174 Ma associated with fluid activity in shear–tensional fractures and/or pores. The P-T conditions of the peak metamorphism were estimated at 4.5 ± 0.5 GPa and 800 ± 50 °C. Retrograde metamorphism recorded conditions of 1.0 GPa and 710 ± 30 °C during the exhumation and cooling process. The mineral transformation from early high-Al clinopyroxene to garnet and to late diopside records the general metamorphic evolution during subduction and exhumation, respectively. One zircon U–Pb analysis presents the Palaeoproterozoic age of 1817 ± 40 Ma, which is coeval with widespread magmatic and metamorphic events in the North China Craton.

Keywords: Sulu orogenic belt; ultrahigh-pressure; garnet clinopyroxenite; metamorphic evolution; zircon U–Pb geochronology

1. Introduction

Following the first discovery of the ultrahigh-pressure (UHP) SiO_2 polymorph coesite in crustal metamorphic rocks [1,2], many other UHP metamorphic indicators have been found in eclogites or garnet peridotites from UHP terranes worldwide [3–10]. UHP metamorphic rocks record evidence of lithospheric subduction and exhumation processes driven by plate collision or mantle convection, and provide natural samples to investigate different types of interactions that occur between the lower crust and mantle [11–17].

The Triassic Dabie–Sulu collision zone located between the Sino–Korean boundary and Yangtze Craton is the world's largest UHP orogenic belt, with an areal extent of >30,000 km^2. Pyroxenites are ubiquitous in the Dabie–Sulu UHP orogenic belt, and may represent an important source of magma in the upper mantle. Therefore, the petrogenesis, tectonic setting, and geodynamic evolution of orogenic belt pyroxenites have become a focus of research. Garnet pyroxenites in the Dabie–Sulu UHP orogenic belt comprise two types: (1) lenses or thin layers in mantle peridotite, such as garnet peridotites in Xugou and Yangkou areas [18]; (2) parts of cumulate igneous bodies that originated from magmatic differentiation, which comprise mainly crustal mafic–ultramafic rocks, such rocks as in the Bixiling area [8].

The Sulu UHP terrane forms the eastern part of the Dabie–Sulu collision zone between the North China and Yangtze cratons, and consists of UHP, very high-pressure (VHP), and HP zones separated by ductile shear zones (Figure 1). These rocks are unconformably overlain by Jurassic clastic strata and Cretaceous volcanic–sedimentary rocks and intruded by post-orogenic Mesozoic granites [19,20]. Coesite-bearing eclogite and related ultramafic rocks usually occur in the surrounding gneisses as lenses or layers, which were initially regarded as being allochthonous. However, coesite inclusions in zircons are also found in gneisses from the Sulu UHP terrane, indicating that the whole orogenic belt experienced UHP metamorphism [21]. Studies of garnet clinopyroxenite in the Hujialin area of the Sulu UHP orogenic belt were carried out in order to understand the petrogenesis and metamorphic evolution of these rocks [8,22–28]. Hiramatsu and Hirajima [22] divided the metamorphic evolution of the Hujialin garnet clinopyroxenites into three stages, and calculated a peak metamorphic temperature of 740 °C with pressures above 2.5 GPa. Chen et al. [23] suggested there were at least two episodes of exsolution, based on the microstructure of amphibole and ilmenite exsolutions in clinopyroxene from the garnet clinopyroxenites, and obtained peak metamorphic pressures of 8 GPa. Zhang et al. [18,24] considered that the Hujialin garnet clinopyroxenites may have formed at 1400 °C and P > 15 GPa. Yang [26] conducted a detailed study of Ca-rich garnet clinopyroxenites from the Hujialin area, and proposed that the Ca-rich garnet clinopyroxenite might have been derived from spinel clinopyroxenite. Zhao et al. [29] also studied the rocks in this area and determined that the Hujialin garnet clinopyroxenites experienced four stages of metamorphic evolution, and obtained a zircon U–Pb age of 215 ± 2 Ma for the UHP metamorphism. However, the nature of the protolith, peak metamorphic conditions, and metamorphic evolution of the Hujialin garnet clinopyroxenite are still controversial. In this paper, we present detailed petrographic, mineralogical, zircon age dating, and phase equilibrium modeling results for the Hujialin garnet clinopyroxenites, and discuss their petrogenesis and metamorphic history.

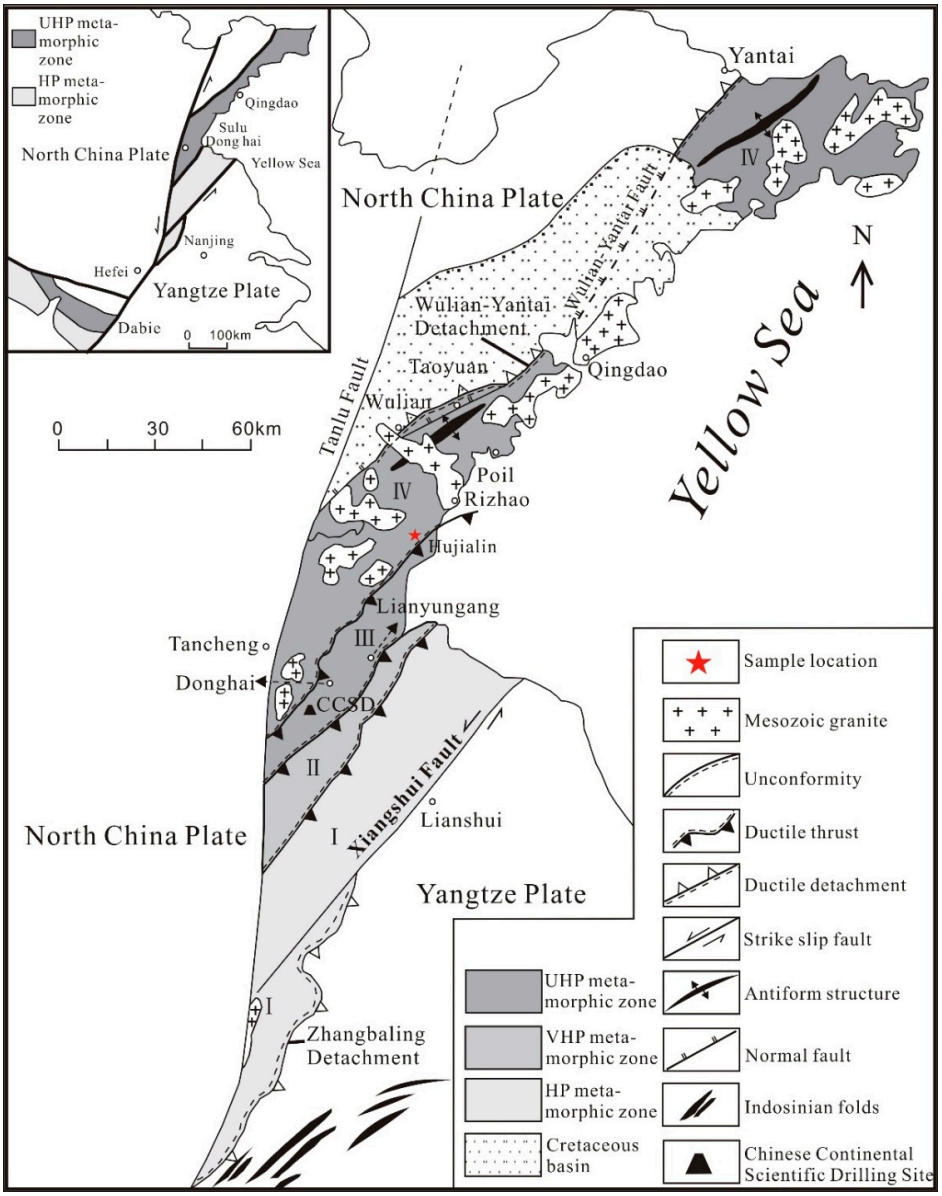

Figure 1. Geological sketch map of Sulu belt (after Xu et al., 2006) [19].

2. Geological Setting

The Sulu UHP orogenic belt is the eastern part of the Triassic Dabie–Sulu orogenic belt, and is bounded by the Tanlu Fault in the west. The Jiashan–Xiangshui and Wulian–Yantai faults constitute its southern and northern boundaries adjacent to the Yangtze and Sino–Korean plates, respectively. The Hujialin area is situated in Rizhao City, Shandong Province, and is located in the middle of the Sulu UHP–HP orogenic belt. The rock unit (i.e., the No. 8 rock body) is ca. 6 km long and trends NNW–SSE. This rock unit is cut by a NE–SW-trending fault (Figure 2). The collected samples are all from the northern rock unit, and garnet pyroxenite can be observed in the upper part of the quarry outcrop in contact with dunite in the lower part. The transverse contact relationship between peridotite and pyroxenite described in previous studies [18,26] is only observed locally. In generally, the pyroxenite lies above the dunite and they tectonically constitute a synform (Figure 3a).

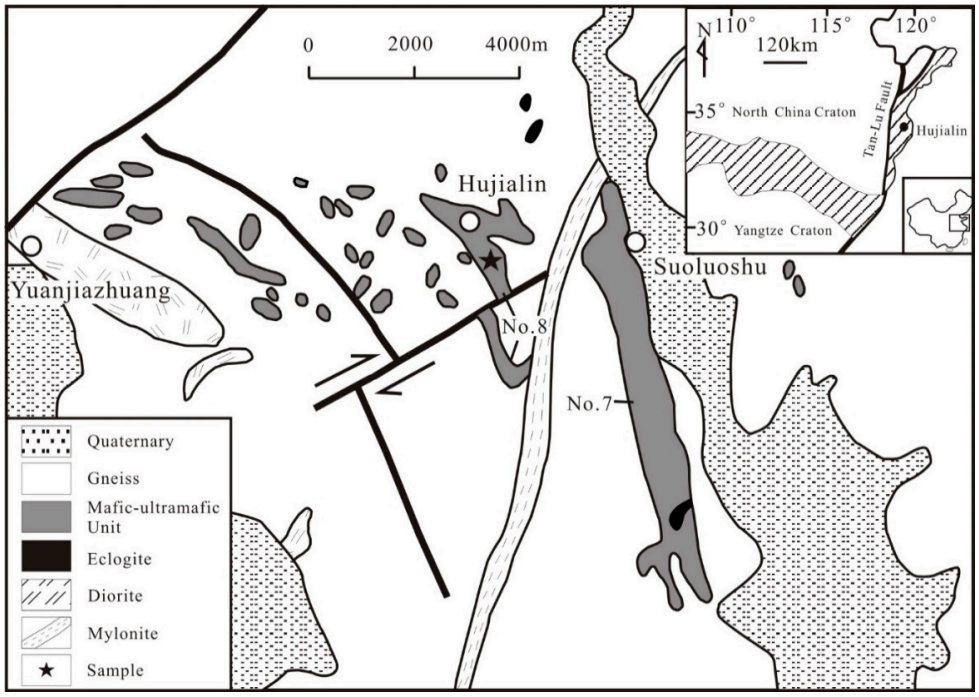

Figure 2. Geological map of the Hujialin area of Rizhao (after Gao et al., 2015) [30].

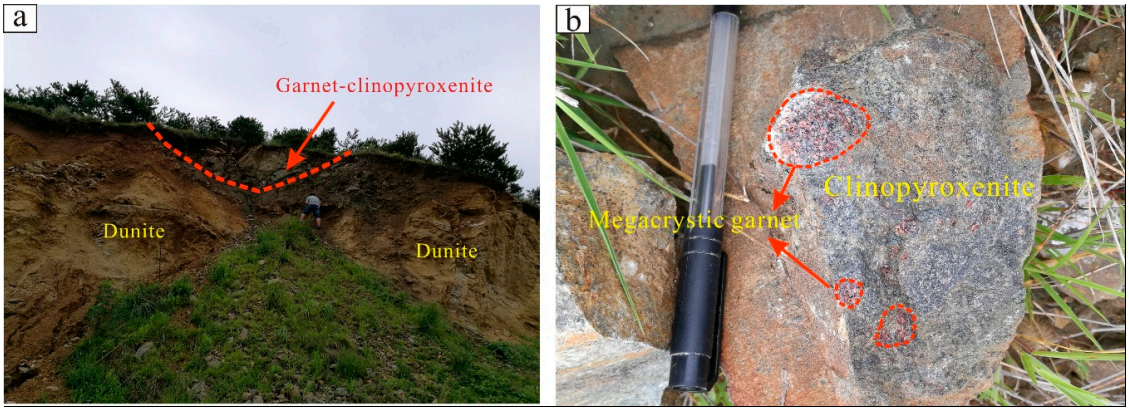

Figure 3. (**a**) Field relations of the Garnet-clinopyroxenite; (**b**) Hand specimen of megacrystic garnet-clinopyroxenite.

3. Analytical Methods

Whole-rock major element contents were analyzed using an X-ray fluorescence (XRF) spectrometer at the Shandong Provincial Bureau of Geology and Mineral Resources Analysis Technology, Shandong, China. Sixteen major and minor elements were determined by wavelength dispersive XRF spectrometry (method GB/T 14506.28-2010) (Table S1).

Garnet and other rock-forming minerals were analyzed with a JEOL JXA-8230 electron probe micro-analyzer (EPMA) at the State Key Laboratory of Marine Geology, Tongji University, Shanghai, China. The operating conditions were: 15 kV accelerating voltage; 10 nA beam current; 0–5 μm beam diameter. Natural and synthetic mineral standards (SPI) and ZAF corrections were used to calibrate all the quantitative analyses.

U–Pb dating and trace element analyses of zircon were simultaneously conducted by laser ablation–inductively coupled plasma–mass spectrometry (LA–ICP–MS) at the Wuhan Sample Solution Analytical Technology, Wuhan, China. Detailed operating conditions for the LA–ICP–MS system and data reduction are the same as those described by Zong et al. [31]. Laser sampling was performed using a

GeolasPro laser ablation system that consists of a COMPexPro 102 ArF excimer laser (wavelength = 193 nm; maximum energy = 200 mJ) and a MicroLas optical system. An Agilent 7700e ICP–MS instrument was used to acquire the ion signal intensities. Helium was used as a carrier gas. Argon was used as the make-up gas, and mixed with the carrier gas via a T-connector before entering the ICP. A signal smoothing device is included in this laser ablation system. The spot size and frequency of the laser were set to 32 μm and 6 Hz, respectively. Zircon 91500 and glass NIST610 were used as external standards for U–Pb dating and trace element calibration, respectively. Each analysis incorporated a background acquisition of ca. 20–30 s, followed by 50 s of data acquisition during ablation. The Excel-based software ICPMSDataCal was used to perform off-line data selection, integration of background and ablation signals, time-drift corrections, and quantitative calibrations for the trace element analysis and U–Pb dating [32]. Concordia diagrams and weighted-mean calculations were performed using Isoplot/Ex_ver3 [33].

4. Petrography and Mineral Chemistry

The rock samples can be divided into three types: Equigranular garnet, porphyroclastic garnet, and megacrystic garnet pyroxenites (Figure 3b). The porphyroclastic garnet pyroxenite is randomly distributed in a narrow strip in the fine-grained garnet pyroxenite, and garnet megacrysts are only found sporadically in the western part of the rock unit. These three types of garnet clinopyroxenite have a similar mineral composition, including clinopyroxene, garnet, ilmenite, magnetite, and minor retrograde amphibole, chlorite, and spinel. Some samples also contain olivine, humite, and clinochlore.

Garnet generally occurs as irregularly shaped megacrysts or porphyroclasts in the pyroxenites, but in the matrix small euhedral grains are also scattered amongst the equigranular diopside aggregates (Figure 4a–d). In some of the porphyroclastic clinopyroxene, the excluded garnet lamellae can be seen (Figure 4e). The garnet consists mainly of grossular and pyrope components (Table S2; Figure 5a). There is a subtle change in the composition of the end-members in the porphyroclastic grain in the studied sample (Figure 6). On one side of the garnet cross-section, the grossular component increased sharply in the rim, the pyrope component decreased simultaneously, and the almandine and andradite components did not change significantly, similar to observations reported by Hiramatsu and Hirajima [22]. The core and rim of the porphyroclastic garnet shown in Figure 6 have average compositions of $Prp_{0.35–0.29}Alm_{0.22–0.15}Gro_{0.50–0.43}Spe_{0.07–0.03}$; the outermost layer has an average composition of $Prp_{0.33–0.27}Alm_{0.14–0.12}Gro_{0.46–0.41}$ $Spe_{0.04–0.03}$. These characteristics indicate that the outermost layer experienced metamorphic replacement rather than a metamorphic growth process from core to rim. This is consistent with the porphyroclastic garnet typically being in relic form (Figure 4c). In addition, the Si content of porphyroclastic garnet is generally >3.0 apfu. Zhang et al. (2003) obtained a similar content for garnet, particularly in a sample of megacrystic garnet-bearing clinopyroxenite. The high garnet Si contents imply that the Hujialin garnet clinopyroxenite experienced UHP metamorphism [18].

Clinopyroxene occurs mainly as porphyroclast, matrix and inclusions in the megacrystic garnet. (Figure 4a,c–e). The chemical compositions of clinopyroxene are listed in Table S3. In the Wo–En–Fs diagram, data for all clinopyroxene is plotted in the diopside field (Figure 5b). The fine-grained clinopyroxene in the matrix is chemically zoned, and the diopside has a constant X_{Mg} ($Mg/[Mg + Fe^{2+}]$) of 0.91–0.99, and contains a small amount of Al_2O_3 (0.86–3.1%) and Na_2O (0.42–0.98%; Table S3). The porphyroclastic clinopyroxene is diopside with X_{Mg} of 0.92–0.95, and an $A1_2O_3$ content that decreases from the core (up to 3.1%) to the rim (ca. 1.5%). Some of the clinopyroxene surrounded by chlorite in the matrix shows component zoning. For example, X_{Mg} decreases from the core (0.94) to rim (0.79–0.83), and $A1_2O_3$ contents increase from the core to rim. Al_2O_3 contents of the clinopyroxene inclusions in the porphyroclastic garnets (2.6–3.1%) are distinctly higher than those of the porphyroclastic (1.45–1.87%) and matrix clinopyroxene (0.74–1.82%). In a Si–Al diagram, the three types of clinopyroxene have different data patterns. Data for clinopyroxene inclusions tend to show a

negative correlation, whereas the other data, especially in the matrix, are relatively clustered, implying that clinopyroxene in the matrix is equilibrated (Figure 7).

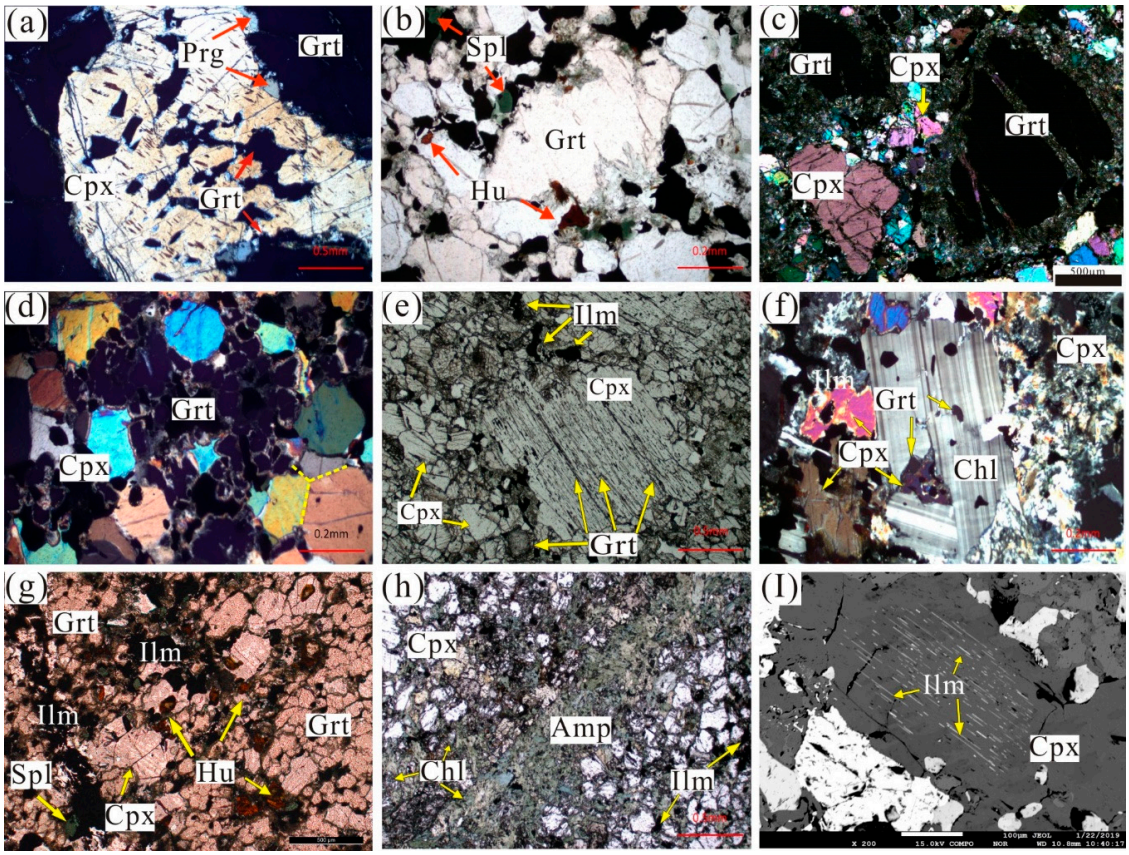

Figure 4. Photomicrograph and backscattered electron images of the Hujialin garnet- clinopyroxenite. (**a**) Megacrysts garnet and clinopyroxene inclusions with pargasite in between forming an intergrowth texture; (**b**) Porphyroclastic garnet associated with diopside, spinel and humite; (**c**) Clinopyroxene and garnet porphyroclast surrounded by fine grained diopside and ilmenite; (**d**) Newly formed anhedral Cpx within fragmented garnet porphyroclast and developed equilibrium structures; (**e**) Garnet lamellae developed in clinopyroxene porphyroclast; (**f**) Late clinochlore showing polysynthetic twinning, including relic subhedral garnet grains; (**g**) Fine grained garnet clinopyroxenite with assemblage of spinel, humite and ilmenite; (**h**) Retrograde amphibole and chlorite developed along the shearing fractures; (**i**) Backscattering image of ilmenite exsolution in clinopyroxene. Mineral abbreviations according to Whitney and Evans (2010) [34].

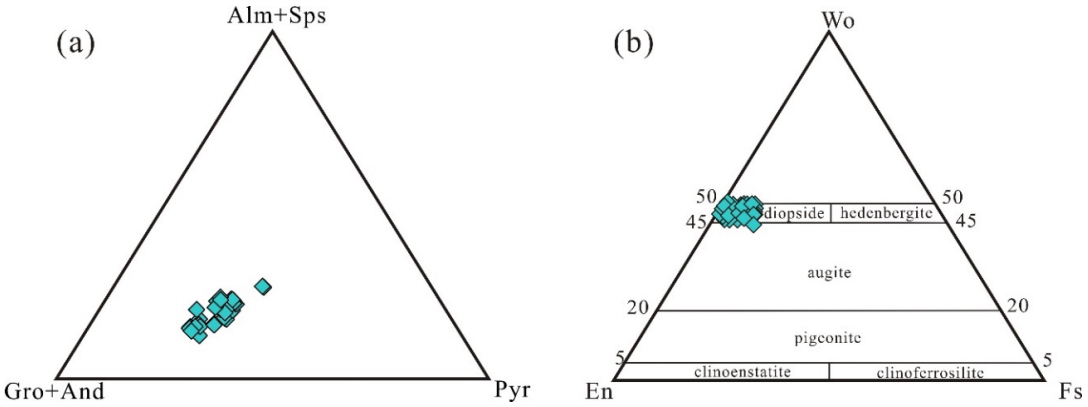

Figure 5. (**a**) Ternary plot of garnet end-member; (**b**) Ternary plot of Wo–En–Fs for clinopyroxene.

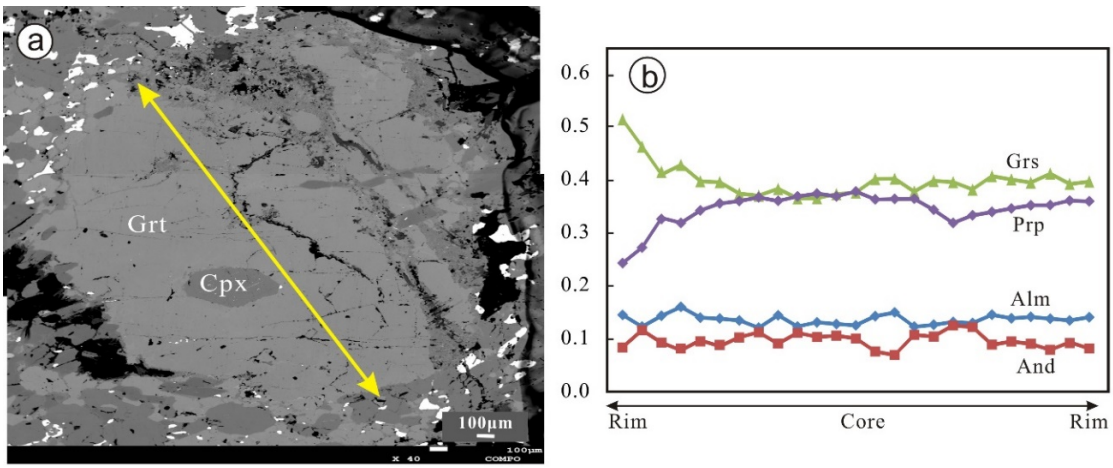

Figure 6. (**a**) BSE image of the garnet porphyroclast, (**b**) cross section diagram showing the compositional zoning of garnet from the Hujialin garnet-clinopyroxenite.

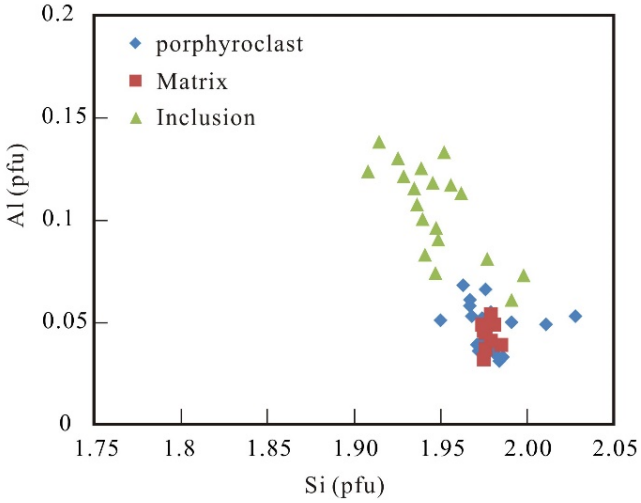

Figure 7. Si versus Al diagram for clinopyroxene.

In addition, some fine-grained garnet, ilmenite, magnetite, and pargasite inclusions are also present in clinopyroxene (Figure 4e,i and Figure 8). In the studied clinopyroxene, ilmenite lamellae formed by exsolution is common, and is cut by exsolved pargasite (Figure 8b,d).

Most of the ilmenite associated with garnet and clinopyroxene is anhedral, and a small amount of ilmenite is present as exsolution lamellae within clinopyroxene (Figure 4g–i). The two groups of ilmenite can be discriminated by their Mg and Mn contents (Table S4): High-Mg and high-Mn groups. The high-Mg ilmenite is usually associated with green spinel in the matrix of the porphyroclastic garnet pyroxenite, and the high-Mn ilmenite occurs mostly in the equigranular garnet pyroxenite.

Spinel is anhedral and looks green in transmitted light. It often associates with ilmenite (Figure 4b,g). The spinels in this study have very low Cr/(Cr + Al) ratios, similar to those reported by Zhang et al. [25] (<0.2), and the Mg/(Mg + Fe^{2+}) ratio is between 0.45 and 0.60 (Table S5). The Ti contents of the spinel are extremely low, and it is possible that during the retrograde process, Ti in the spinel entered the accompanying ilmenite.

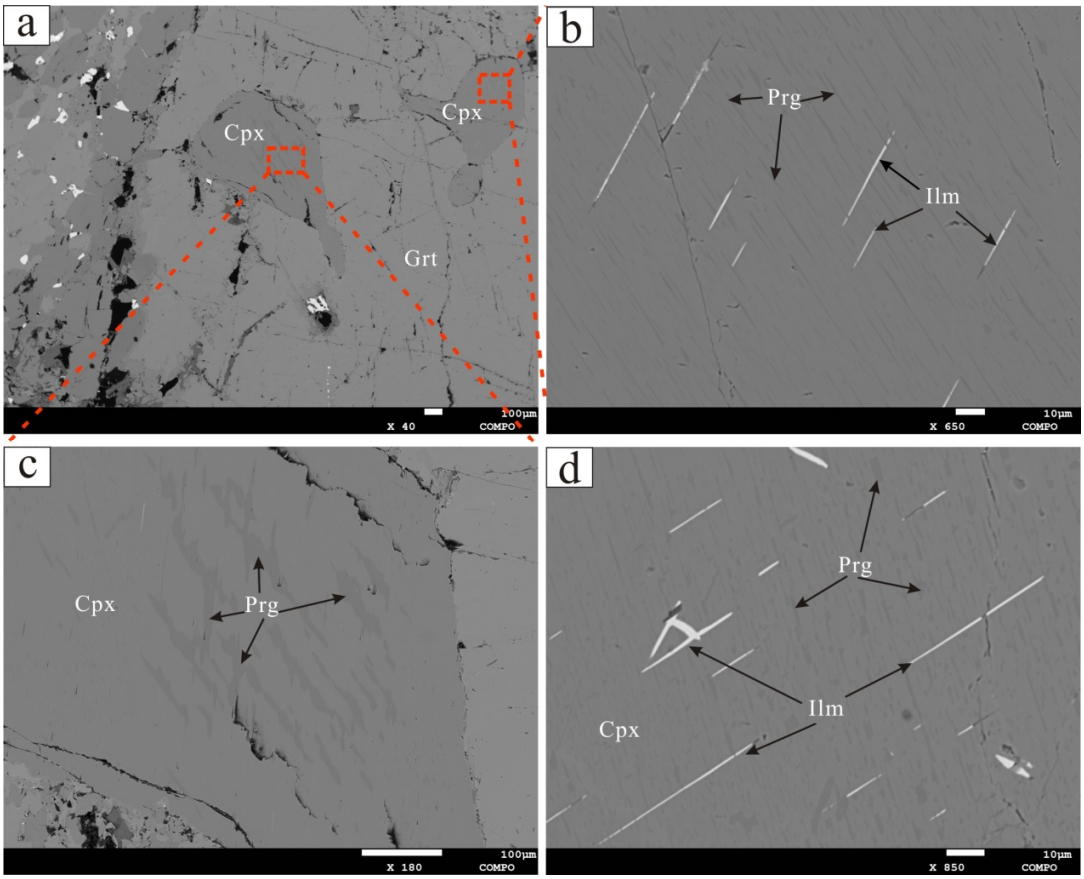

Figure 8. Backscattered images of (**a**) clinopyroxene inclusions in garnet porphyroclast, (**b**) exsolved Prg and Ilm in clinopyroxene, (**c**) exsolved Prg in clinopyroxene and (**d**) exsolved Prg and Ilm in clinopyroxene.

The amphibole can be divided into two types (Figure 9), which are pargasite and edenite. Amphibole occurs in three different microtextural contexts: (1) inclusions in porphyroclastic garnet; (2) exsolution lamellae in clinopyroxene included in porphyroclastic garnet (Figure 8b–d); (3) small grains spatially related to garnet rims (Figure 4a). The edenite is mainly a retrograde phase within amphibole-rich bands in the pyroxenite samples (Figure 4h). The Al^{IV} content (1.60–1.95) of pargasite is higher than that of edenite (1.20–1.45), and both have a high $Mg/(Mg + Fe^{2+})$ ratio (0.83–1.00). A Na–Si plot (Figure 9c) shows that the Si contents of pargasite inclusions in garnet are significantly lower than those of the pargasite in the matrix. In a K–Si plot (Figure 9d), there is a positive correlation between the K and Si contents of pargasite inclusions and matrix pargasite. These pargasites occur mainly as inclusions in garnet or in the matrix associated with clinopyroxene, and its Na_2O content (1.45–2.53%) is slightly lower than that of pargasite exsolved in clinopyroxene (2.86–3.64%), and similar to the Na_2O content (1.77–2.45%) of pargasite in the Lizard Complex lherzolite [35]. The clinopyroxene-exsolved ilmenite lamella shown in Figure 4i exhibit a strong crystallographic orientation. Figure 4a shows the exsolution texture of clinopyroxene inclusions in megacrystic garnet. The exsolved minerals are mainly amphibole and ilmenite, and the two minerals are mutually cut by each other. Chen and Xu [23] reported similar observations for clinopyroxene from the Hujialin area, whereby acicular ilmenite cuts pargasite lamellae, indicating that exsolution of ilmenite occurred later than that of pargasite. This shows that the Hujialin garnet clinopyroxenite experienced at least two metamorphic events during exhumation and decompression.

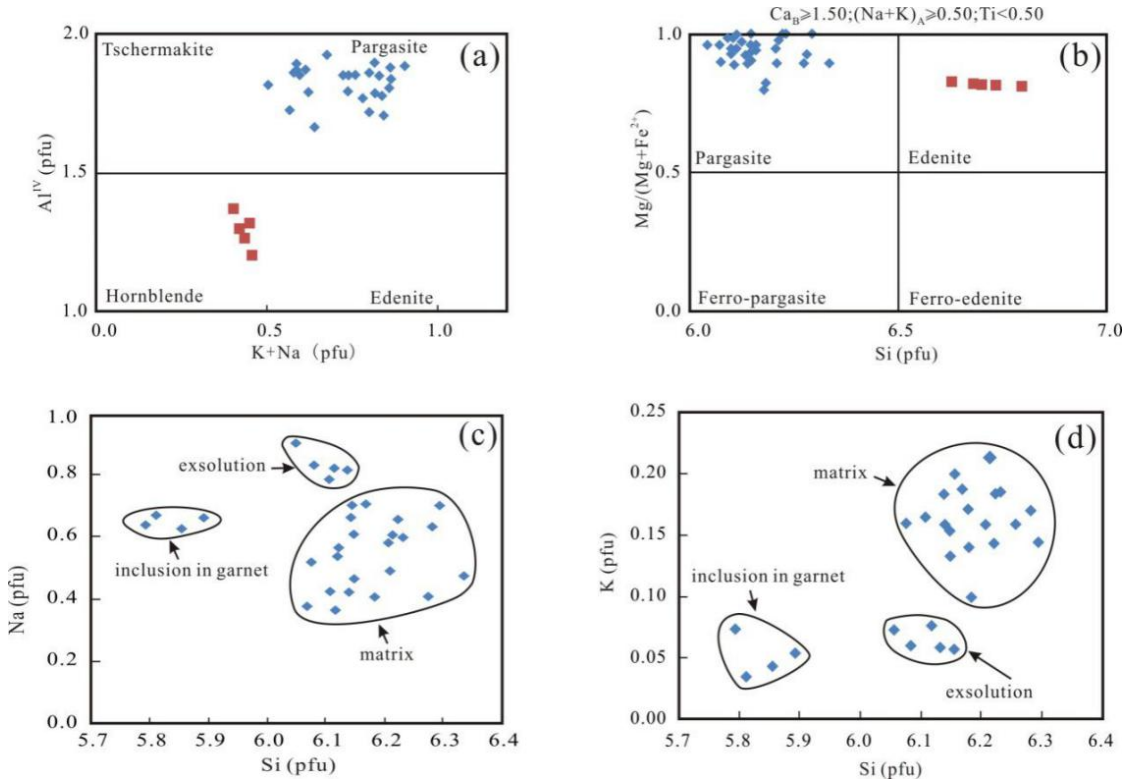

Figure 9. (**a**,**b**) Diagram of amphibole composition in two groups; (**c**,**d**) Si-Na and Si-K diagrams of pargasites as inclusions in Grt, exsolutions in Cpx and fine grains in the matrix.

Two chlorites were found in sample RZ-1; one is a clinochlore with polysynthetic twinning (Figure 4f) and the other is retrograde chlorite (Figure 4h). There are differences in the compositions of the two chlorites (Table S6). Al_2O_3 and MgO contents of the clinochlore are slightly higher than those of the chlorite, while FeO contents are significantly lower in the clinochlore. This indicates that the two chlorite generations reflect different metamorphic events. Numerous well-formed clinochlore crystals is surrounded by small grains of garnet, clinopyroxene, ilmenite, spinel, and other minerals (Figure 4f). Clinochlore can be stable at HP and survive UHP metamorphism, as evidenced by the reaction clinochlore = forsterite + pyroxene + H_2O at pressures of up to 3.5 GPa [36,37]. Clinochlore is the primary water transporting mineral in subduction zones, and may be the only aqueous phase present above the decomposition temperature of serpentine [38]. When clinochlore eventually breaks down, it contributes a large amount of water to the subduction zone [39].

Olivine was rarely recognized in the studied samples, and a very small amount of olivine was found during electron microprobe analysis in the matrix or as inclusions in clinopyroxene. A small amount of humite was also found in sample RZ-1 (Figure 4b,g), with ilmenite surrounding reddish brown humite. The humite contains mainly SiO_2 (34–41%), FeO (16–23%), and MgO (40–42%) (Table S6). The Al_2O_3 and CaO contents are extremely low and the TiO_2 contents are negligible. In the Sulu UHP metamorphic terrane, Yang [40] reported garnet pyroxenite and eclogite containing Ti-clinohumite, which is mainly present between garnet and pyroxene. The garnet and orthopyroxene combined with Ti-clinohumite typically record a pressure condition of >4.5 GPa, indicating UHP conditions [41]. However, the humite TiO_2 content in the studied sample was extremely low, indicating that Ti was consumed during exhumation after UHP metamorphism by surrounding ilmenite (Figure 3g).

5. Whole-Rock Geochemistry

5.1. Major Elements

The analysis results of the major elements of the garnet pyroxenite samples in Hujialin are shown in Table S1. Samples RZ-1 and RZ-2 are collected near the megacrystic garnet pyroxenite, which is rich in garnet porphyroclasts and labeled as garnet-rich porphyroclastic pyroxenite. Samples RZ-5, 6, 8, and 14 are categoried to porphroclastic garnet pyroxenite. Sample RZ-11 is equigranular garnet pyroxenite, enriched in pyroxene. It can be seen that the three types of samples show slight differences in the composition of major elements. The content of MgO (12.98%), SiO_2 (53.88%) and TiO_2 (0.73%) in equigranular garnet pyroxenite is slightly higher than that of porphyroclastic garnet clinopyroxenite MgO (9.32–11.0%), SiO2 (42.41–51.66%) and TiO_2 (1.39–1.76%). The samples have relatively high CaO/Al_2O_3 (2.85–3.05), low $MgO/(MgO + FeO^T)$ (0.62–0.51), and have a similar composition as large clinopyroxene crystals, plus exsolved garnet in eclogite xenoliths from kimberlite analyzed by Zhang et al. [18], which suggests their protolith may have been a pyroxenite [42,43].

5.2. Trace Elements

Trace element data for the three types of garnet clinopyroxenites are listed in Table S1 and shown in Figure 10a,b. The garnet clinopyroxenites have similar convex-upward rare earth element (REE) patterns, with light REE enrichment and heavy REE depletion. Given that heavy REEs partition strongly into garnet, the depleted heavy REE pattern of the garnet clinopyroxenites indicate that their protolith was garnet-free. Trace element patterns (Figure 10b) show that the three types of rock have some similarities, but also significant differences. The samples have large positive Pb anomalies and depletions in high-field-strength elements (HFSEs; e.g., Nb and Ti), suggestive of fluid metasomatism [28].

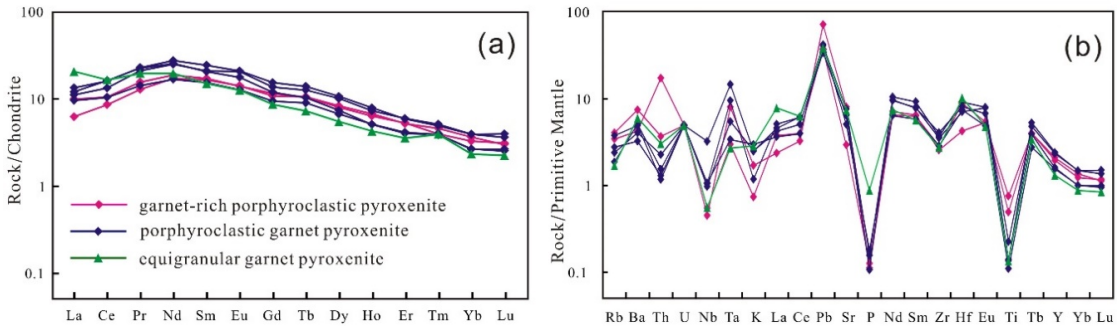

Figure 10. (**a**) Chondrite normalized REE patterns for the Hujialin garnet-clinopyroxenites; (**b**) Primitive mantle-normalized incompatible element spidergrams for the Hujialin sample (normalized values are from McDonough and Sun, 1995) [44].

6. U–Pb Geochronology

Two garnet clinopyroxenite samples (18RZ-1-1 and 18RZ-1-3) were U–Pb dated, which yielded five groups of ages (Table S7, Figure 12): (1) 1824 ± 40 Ma, (2) 753.0 ± 9.8 Ma, (3) 350.0 ± 3.9 Ma, (4) 215.0 ± 5.7 Ma, and (5) 180.0 ± 2.4 Ma. Zircon cathodoluminescence images (Figure 11) and morphological characteristics identified two types of zircon. The first is compositionally unzoned with Th/U = 0.015–0.081, representing metamorphic zircon. The second has core and rim structures with a strong contrast in cathodoluminescence and Th/U = 0.57–2.20, which are magmatic zircon.

In chondrite-normalized REE diagrams, the magmatic zircon shows obvious positive Ce and negative Eu anomalies and heavy REE enrichment, while the metamorphic zircon has flat heavy REE patterns and no Eu anomalies (Figure 12b).

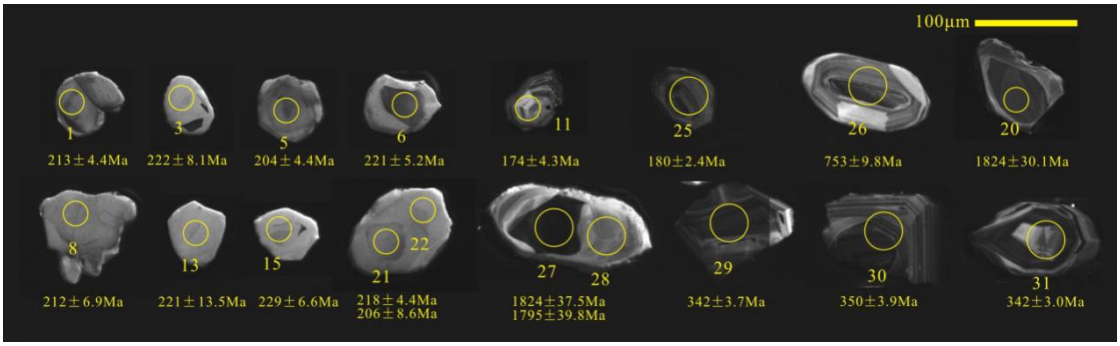

Figure 11. Cathodoluminescence images of representative zircon grains and corresponding U-Pb ages from the garnet-clinopyroxenite samples.

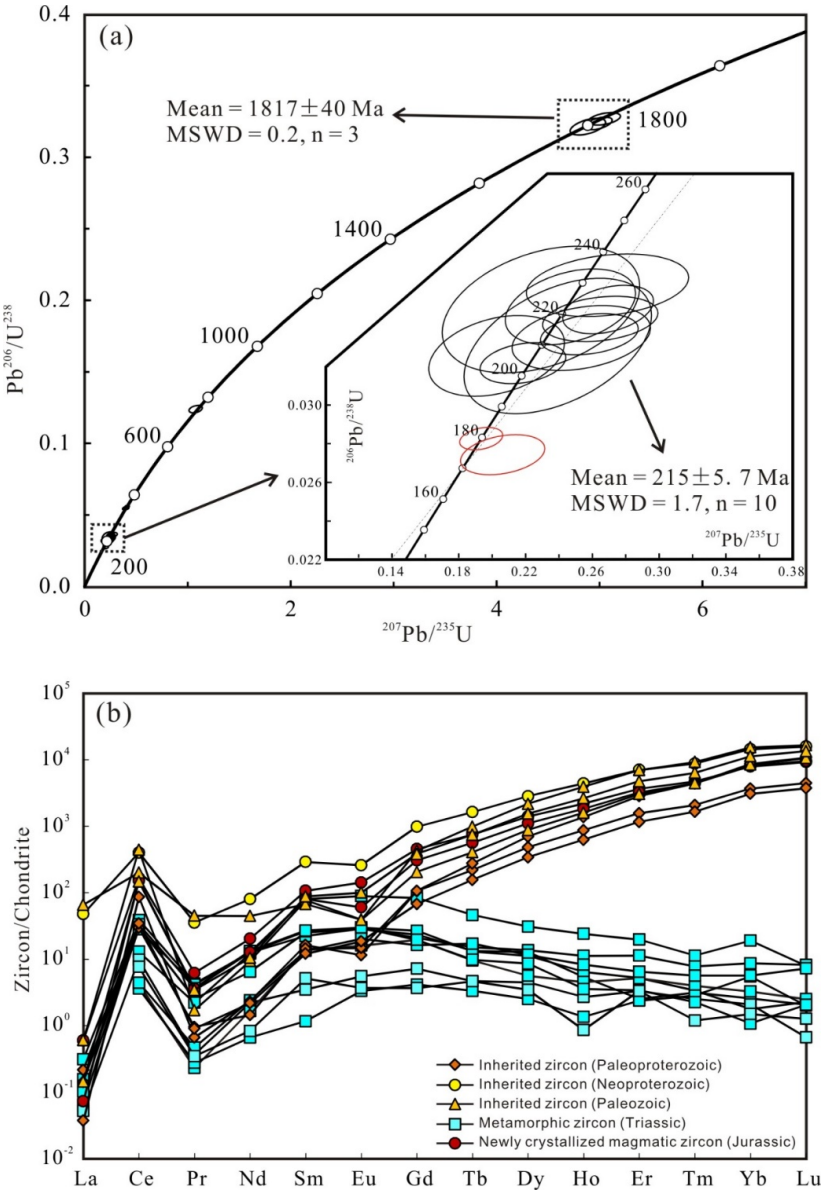

Figure 12. Concordia diagram and U–Pb age (**a**), and corresponding chondrite normalized zircon REE patterns (**b**) for representative garnet-clinopyroxenite (normalization values are from McDonough and Sun, 1995) [44].

The first group of ages from 1824–1795 Ma, with a weighted-mean age of 1817 ± 40 Ma (MSWD = 0.2; n = 3), is coeval with magmatism that occurred during rifting of the Columbia Supercontinent in the North China Craton. This may represent the formation age of the Hujialin garnet pyroxenite, when it crystallized from a magma in the upper mantle or at the crust–mantle boundary [45]. The second group of ages with a weighted-mean of 753.0 ± 9.8 Ma coincides with the formation age of the surrounding gneisses (ca. 780–750 Ma) in the Sulu orogenic belt [46–48]. The third group of ages is from 371–336 Ma. It has been reported [49] that inherited magmatic zircon has a $^{206}Pb/^{238}U$ age of 378 ± 6 Ma in the Weihai garnet peridotite. This type of zircon is not completely recrystallized and has not experienced complete Pb loss. Such age data cannot represent the age of the protolith, and have no geological significance. The fourth group of ages is from 229–204 Ma, with a weighted-mean of 215.0 ± 5.7 Ma (MSWD = 1.7; n = 10). The ages of this fourth group are slightly younger than those of Sulu UHP metamorphism (240–220 Ma) [46–49], and likely records the timing of exhumation after UHP metamorphism. The fifth group of ages is from 180–174 Ma, and records amphibolite-facies retrogression.

7. Discussion

7.1. Metamorphic Evolution

In order to constrain the metamorphic evolution, phase equilibria modeling is necessary. In this paper, Perple_X-6.7.4 software [50,51], combined with the Holland and Powell [52] internally consistent thermodynamic database, was used to construct the *P–T* pseudosection. Major elements of sample RZ-1 (Table S1) were used in the Na_2O–CaO–TiO_2–FeO–MgO–Al_2O_3–SiO_2–H_2O (NCFMASHTO) system for phase equilibria modeling. Because K_2O (0.02%) and MnO (0.11%) do not control any major phase in the rock system, and MnO is only present in garnet, they were ignored in the calculations. In this model, we assumed that the fluid H_2O is saturated, and the pseudosection shown in Figure 13 was calculated using Gt (WPH), Fsp (C1) [52], Ilm (WPH) [53], Cpx (HP) [54], Amph (DHP) [55], Chl (HP), Ep (HP) and Spl (WPC) [56] solution models.

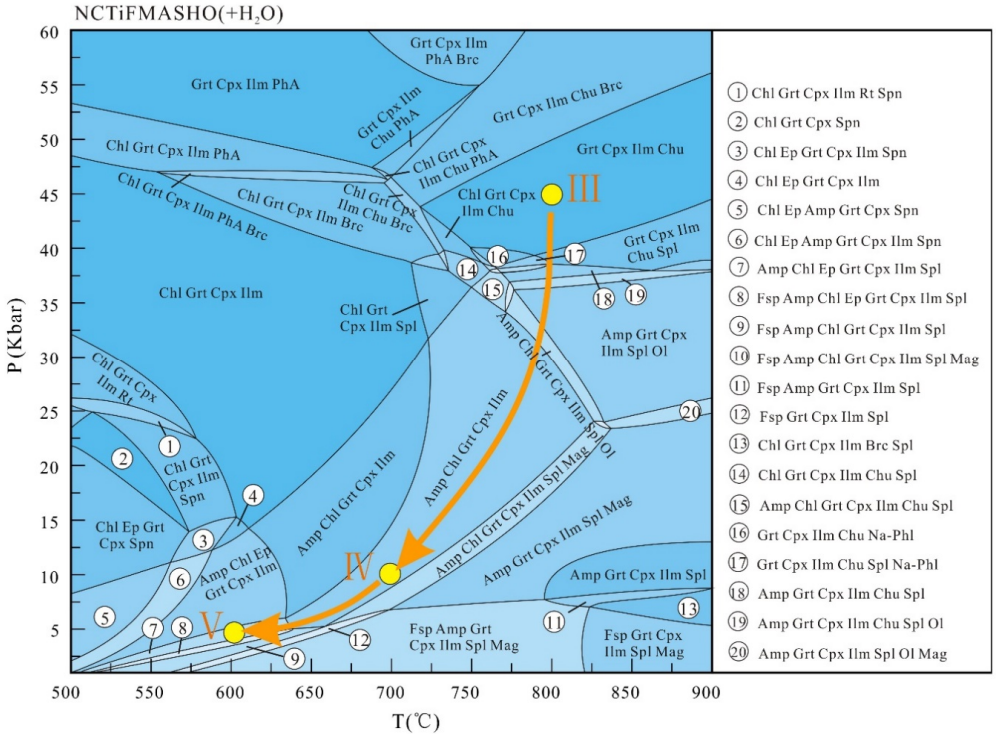

Figure 13. P-T pseudosection from measured bulk composition of sample RZ-1 in the system NCTiFMASHO (H_2O in excess). Compositions used for calculating. P-T pseudosection is listed Table S1. Mineral abbreviations take after Whitney and Evans (2010) [34].

According to the petrography and mineral chemistry, the evolution of the Hujialin garnet clinopyroxenites can be divided into five stages: Stage I = protolith formation; stage II = formation of porphyroclastic garnet pyroxenite accompanying subduction; stage III = formation of porphyroclastic or equigranular garnet clinopyroxenite with a mineral assemblage of Grt + Cpx + Ilm + Hu accompanying exhumation; stage IV = progressive cooling and decompression producing a mineral assemblage of Grt + Cpx + Ilm + Chl + Amp; stage V = late epidote amphibolite-facies retrograde metamorphism producing a mineral assemblage of Gt + Cpx + Amp + Chl + Ep + Ilm.

Protolith formation has been speculatively inferred from petrographic observations of inclusions in garnet porphyroclastics. In general, previous studies have recognized cumulate spinel pyroxenite as being the protolith, which formed in the upper mantle or at the crust–mantle boundary over a *P–T* range of 1–1.5 GPa and >1000 °C for stage I [18,26,29].

In stage II, the exsolved garnet and ilmenite in clinopyroxene (see Figure 4e,i) are regarded as the product of subduction and increasing pressure [18,29]. From the protolith to garnet clinopyroxenite, the primary clinopyroxene must have been transformed to garnet since excluded lamellae occurred in the porphyroclastic clinopyroxene. The reduction of Al content from precusor Cpx to the matix Di is about one half, perhaps due to Al_2O_3 being consumed by garnet as the protolith is converted to megacrystic garnet clinopyroxenite. With increasing pressure, the octahedral Si–Al substitution in garnet was important. In the megacrystic garnet clinopyroxenite, garnet and pyroxene are intergrown forming a massive pegmatite-like rock (Figure 4a). The Si content of porphyroclastic garnet is high, generally >3.0 apfu, implying that the Hujialin garnet clinopyroxenite experienced UHP metamorphism. High-pressure conditions are favorable for garnet formation, due to the difficulty of the Al–Si substitution in the tetrahedral site of the Ca Tschermak component as indicated by [25,26]:

$$CaMgSi_2O_6 + CaAl_2SiO_6 = Ca_2MgAl_2Si_3O_{12} \quad (1)$$

Stages III and IV represent the decomposition of the megacrystic garnet pyroxenite (Figure 13). The metamorphosed ultramafic rocks underwent isothermal decompression or a fluid addition event under high stress conditions, which resulted in dynamic recrystallization. Firstly, the massive garnet was fragmented by stress, creating minute pyroxene aggregates along the edges of small grains of high-Si garnet. Newly formed diopside grains gradually replaced the garnet fragments, leaving behind pophyroclastic garnet surrounded by a clinopyroxene–garnet aggregate, which finally led to the equigranular mineral assemblage in the matrix (Figure 4d). Unlike stage II, high grossular garnet with low Si was produced in stage III, corresponding to a pressure decrease. The reaction for this is as follows [26]:

$$Ca_2MgAl_2Si_3O_{12} + Mg_2SiO_4 = 2CaMgSi_2O_6 + MgAl_2O_4 \quad (2)$$

The mineral assemblage of Grt + Hu + Cpx + Sp (+ Ilm) is shown in Figure 4b, i.e., Ilmenite is associated with Mg–Al spinel in the reaction, but has a high Mg content, unlike the massive spongy ilmenite scattered around the clinopyroxene, with a high Mn content which perhaps resulted from the decomposition of ilmenite-exsolved clinopyroxene.

The geothermometer for garnet–clinopyroxene mineral pairs given by Ravna (2000) [57] was used to calculate temperatures (Table S8):

$$\begin{aligned} T(^\circ C) = [(1939.9 + 3270X_{Ca}^{Grt} - 1396(X_{Ca}^{Grt})^2 + 3319X_{Mn}^{Grt} - 3535(X_{Mn}^{Grt})^2 + 1105X_{Mg\#}^{Grt} - 3561 \\ (X_{Mg\#}^{Grt})^2 + 2324\,(X_{Mg\#}^{Grt})^3 + 169.4P\,(GPa)/(\ln K_D + 1.223)] - 273 \end{aligned} \quad (3)$$

This $K_D = (Fe^{2+}/Mg)^{Grt}/(Fe^{2+}/Mg)^{Cpx}$, $X_{Ca}^{Grt} = Ca/(Ca + Mn + Fe^{2+} + Mg)$, $X_{Mn}^{Grt} = Mn/(Ca + Mn + Fe^{2+} + Mg)$, $X_{Mg\#}^{Grt} = Mg/(Mg + Fe^{2+})$.

The mineral assemblage of stage III in the calculated *P–T* diagram (Figure 13) is Grt + Cpx + Ilm + Hu, which is consistent with the petrographic observations and appear in the *P–T* domain of 4–5 GPa and at ≥750 °C. The calculated temperature of the Ravna [57] garnet clinopyroxenite Fe–Mg

exchange geothermometer is 800 ± 50 °C at 4.5 GPa, and similar to the estimations from phase equilibria modeling. Therefore, the UHP metamorphic stage of the Hujialin garnet clinopyroxenite occurred at 4.5 ± 0.5 GPa and 800 ± 50 °C.

In stage IV, some water-bearing minerals such as clinochlore and amphibole were present, and the zircon U–Pb ages of 215–208 Ma are consistent with the age of granitic magmatism in Yangkou [58,59]. It is thought that deep melting of adjacent granitic rocks contributed to the metamorphism of the Hujialin pyroxenite and were directly related to exhumation. Based on the phase equilibria modeling, amphibole geobarometer of Schmidt [60], and garnet–clinopyroxene geothermometer [57], stage IV *P–T* condition were 1.0 GPa and 710 ± 30 °C (Table S8).

During exhumation and uplift, the garnet clinopyroxenite underwent retrograde epidote amphibolite-facies metamorphism. In sample RZ-1, some of the garnet porphyroblasts were replaced by the secondary minerals Gt + Cpx + Amp + Chl + Ep + Ilm, and some clinopyroxene was also retrograded into amphibole and chlorite aggregates. The amphibole geobarometer of Schmidt [60] and Fe–Mg exchange geothermometer of Ravna [57] yield *P–T* conditions for stage V of 0.5 GPa and 600 ± 30 °C.

7.2. Protolith and Structural Model

Based on petrographic studies, it has been proposed that the Hujialin garnet clinopyroxenite is formed from spinel clinopyroxenite through the exsolution of Ca-rich garnet, magnetite, ilmenite, and Fe spinel in augite [8,18,24,26,61]. The original spinel clinopyroxenite was formed by magmatic differentiation near the crust–mantle boundary [26,28]. The Hujialin garnet clinopyroxenite has high CaO and CaO/Al_2O_3, low Na, light REE enrichment, heavy REE depletion, and low Cr, Co, and Ni contents, consistent with a cumulate clinopyroxenite origin. Most of these data define a compositional trend from high-Mg cumulates to gabbros [62]. The significant depletions in incompatible trace elements (Zr, Y, and heavy REEs) in the garnet clinopyroxenite may also be related to the cumulate nature of the protolith [26]. The light REE enrichment can be attributed to fluid interaction (Figure 10a), and the low Ni and Cr contents and $Mg^{\#}$ values to early olivine crystallization in the magma [28].

The garnet clinopyroxenite samples show relative depletion of HFSEs (e.g., Nb, Zr, and Ti) and relative enrichment of large-ion lithophile elements (e.g., Rb, Sr, Ba, and Pb), which are typical geochemical features of subduction magmatism [63–68]. Most subduction-related UHP peridotites are interpreted to be from the lithospheric mantle wedge, above the pre-subduction zone [69,70], which typically exhibits enrichments of oceanic plate-derived elements [68,71–75]. According to field observations, and petrological and geochemical data, the Hujialin garnet clinopyroxenites are cumulates formed by melt crystallization in the mantle wedge of an ancient subduction zone. Zhang et al. [18] considered that the protoliths were formed in a subduction zone during Triassic continental collision and were recrystallized to form majorite at mantle depths (>450 km), and then underwent decompression exsolution as it ascended to shallow mantle depths [8,18,24,25,60]. The formation age of 1817 ± 40 Ma may correspond to the rifting of the Columbia Supercontinent and the widely distributed mafic dike swarms in the North China Craton [45]. We propose a five-stage tectonic model for the Hujialin garnet clinopyroxenite block in the Sulu UHP orogenic belt (Figure 14). The first stage (1817 ± 40 Ma) involved the rifting of Columbia, resulting in complex crust–mantle processes. The second stage (753.0 ± 9.8 Ma) involved the continental rifting of Rodinia and the generation of large-scale granitic rocks along the margin of the Yangtze Craton (i.e., the present-day gneisses) [19]. The third stage involved subduction of the Yangtze Plate and collision with the North China Craton, which triggered asthenospheric wedge flow and brought the cumulate ultramafic rocks into the subduction channel [9]. The fourth stage (215–206 Ma) involved subduction of granitic continental crust into the mantle, partial melting of the granitic rocks, and exhumation of UHP metamorphic rocks to crustal level. Finally, the UHP orogenic belt was overprinted by retrograde metamorphism.

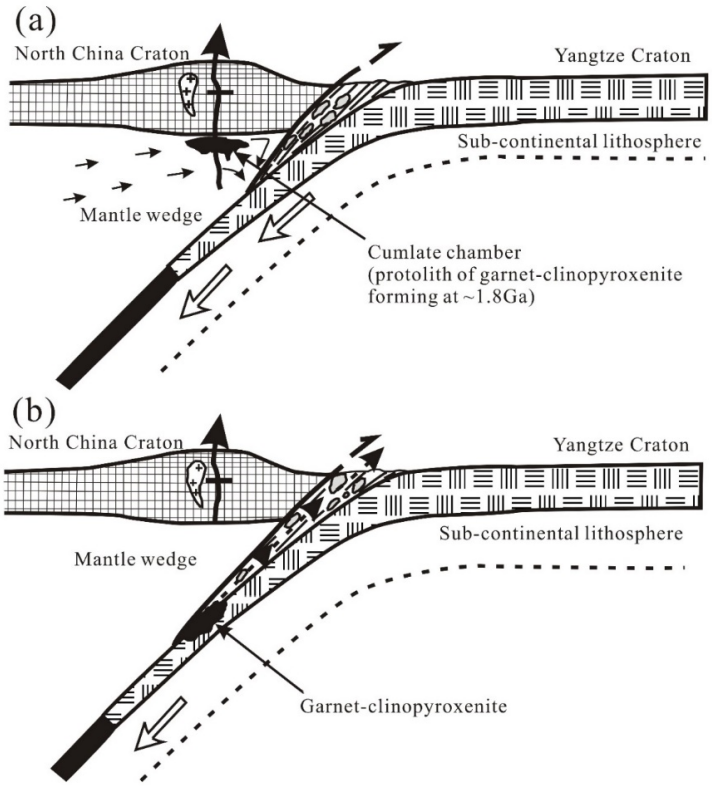

Figure 14. Simplified geodynamic model for illustrating the formation and evolution of the Hujialin garnet-clinopyroxenite. (**a**) Subduction of Yangztze plate before 215 Ma; (**b**) Subduction of Yangztze plate and exhumation of some UHP metamorphic block after 215 Ma.

8. Conclusions

The Hujialin garnet clinopyroxenites had a cumulate spinel clinopyroxenite protolith, with a formation age of 1817 ± 40 Ma. The early subduction process was accompanied by garnet and ilmenite exsolution in pyroxene, which led to the pyroxene becoming enriched in Ca and Mg. Early and late-stage pyroxene have very different Al_2O_3 contents, due to the transformation of clinopyroxene to garnet.

The protolith of garnet clinopyroxenite was carried into the subduction channel by mantle wedge flow, and experienced UHP metamorphism at age of 215.0 ± 5.7 Ma and 4.5 ± 0.5 GPa/800 ± 50 °C. The retrograde minerals were derived from a variety of HP mineral assemblages, which was formed by the decomposition of garnet, which was accompanied by the formation of abundant ilmenite and Ca-rich pyroxene. The cooling and decompression of subducted garnet clinopyroxenites associated with the retrogressive metamorphism at the age of 206 Ma and 1.0 GPa and 710 ± 30 °C.

The enrichment of light REEs and LILEs and depletion of heavy REEs and HFSEs support the hypothesis that the protolith garnet clinopyroxenites were derived from the mantle wedge that had been contaminated by fluids from the subducting crust. The mantle wedge is becoming an important source of fluid and gold for the orogenic gold deposits of the giant Jiaodong gold province in the North China Craton [76].

Supplementary Materials: The following are available online at http://www.mdpi.com/2075-163X/10/3/225/s1, Table S1: Major element oxides (wt%) and trace element (ppm) compositions of the Hujialin garnet- clinopyroxenites, Table S2: EPM analyses of representative garnet compositions, Table S3: EPM analyses of representative clinopyroxene compositions (inc-clinopyroxene inclusions in garnet), Table S4: EPM analyses of representative ilmenite and magnetite, Table S5: EPM analyses of representative amphibole and spinel (exs-exsolution of pargasite in clinopyroxene), Table S6: Representative compositions of chlorite, humite and olivine, Table S7: U–Pb isotopic dating result for zircons from the Hujialin garnet-clinopyroxenite, Table S8: Garnet-clinopyroxene P-T estimate according to Krogh Ravna (2000) [56].

Author Contributions: Conceptualization, Z.W., X.-P.L. and S.W.; methodology, Z.L., D.L., Y.Y.; software, S.Z., S.W.; validation, Z.W., X.-P.L. and J.W.; formal analysis, S.Z.; investigation, Z.W., S.Z., X.-P.L., J.L., F.-M.K.; resources, X.-P.L., S.W.; data curation, S.Z., S.W.; writing —original draft preparation—Z.W., S.Z.; writing—review and editing, Z.W., X.-P.L.; visualization, S.Z., D.W.; supervision, Z.W., X.-P.L.; project administration, X.-P.L., F.-M.K.; funding acquisition, X.-P.L., S.W. All authors have read and agreed to the published version of the manuscript.

Funding: This research was supported by the National Natural Science Foundation of China (Grants U1906207 and 41472051) and the NSFC/NRF Research Cooperation Program (Grant 41761144061).

Acknowledgments: We thank Zhonghua Tian for his helpful discussions and assistance during the writing of this paper. We thank van Roermund H.L.M. for his field discussion and Yang Li for helping with the drawing. We would also like to thank two anonymous reviewers for their constructive and thoughtful comments that are helpful in improving the paper.

Conflicts of Interest: The authors declare no conflict of interest.

References

1. Chopin, C. Coesite and pure pyrope in high-grade blueschists of the Western Alps: A first record and some consequences. *Contrib. Mineral. Petrol.* **1984**, *86*, 107–118. [CrossRef]
2. Smith, D.C. Coesite in clinopyroxene in the Caledonides and its implications for geodynamics. *Nature* **1984**, *310*, 641–644. [CrossRef]
3. Sobolev, N.V.; Shatsky, V.S. Diamond inclusions in garnets from metamorphic rocks-a new environment for diamond formation. *Nature* **1990**, *343*, 7427–7446. [CrossRef]
4. Yang, J.J.; Godard, G.; Kienast, J.R.; Lu, Y.Z.; Sun, J.X. Ultrahigh-pressure (60 kbar) magnesite-bearing garnet peridotites from Northeastern Jiangsu, China. *J. Geol.* **1993**, *101*, 541–554. [CrossRef]
5. Yang, J.J.; Zhu, H.; Deng, J.F.; Zhou, T.Z.; Lai, S.C. Discovery of garnet peridotite atthe northern margin of the Qaidam Basin and its significance. *Acta Petrol. Mineral.* **1994**, *13*, 97–105.
6. Dobrzhinetskaya, L.F.; Eide, E.A.; Larsen, R.B.; Sturt, B.A.; Tronnes, R.G.; Smith, D.C.; Posukhova, T.V. Microdiamond in high-grade metamorphic rocks of the Western Gneiss Region, Norway. *Geology* **1995**, *23*, 597–600. [CrossRef]
7. Van Roermund, H.L.M.; Drury, M.R. Ultra-high pressure (P > 6 GPa) garnet peridotites in Western Norway: Exhumation of mantle rocks from >185 km depth. *Terra Nova* **1998**, *10*, 295–301. [CrossRef]
8. Zhang, R.Y.; Liou, J.G.; Yang, J.S.; Yui, T.F. Petrochemical constraints for dualorigin of garnet peridotites from the Dabie-Sulu UHP terrane, eastern-central China. *J. Metamorph. Geol.* **2000**, *18*, 149–166. [CrossRef]
9. Song, S.G.; Zhang, L.F.; Niu, Y.L. Ultra-deep origin of garnet peridotite from theNorth Qaidam ultrahigh-pressure belt, Northern Tibetan Plateau, NW China. *Am. Mineral.* **2004**, *89*, 1330–1336. [CrossRef]
10. Zhang, C.; van Roermund, H.; Zhang, L.F. Orogenic garnet peridotites: Tools to reconstruct Paleo-Geodynamic settings of fossil continental collision zones. *Ultrah. Press. Metamorph.* **2011**, 513–551. [CrossRef]
11. Pearson, D.G.; Davies, G.R.; Nixon, P.H. Geochemical constrains on the petrogenesis of Diamond Facies Pyroxenites from the Beni Bousera Peridotite Massif, North Morocco. *J. Petrol.* **1993**, *34*, 125–172. [CrossRef]
12. Li, X.-P.; Yan, J.-Y.; Schertl, H.-P.; Kong, F.-M.; Xu, H. Eclogite from the Qianliyan Island in the Yellow Sea: A missing link between the mainland of China and the Korean peninsula. *Eur. J. Mineral.* **2014**, *26*, 727–741. [CrossRef]
13. Pilitsyna, A.V.; Tretyakov, A.A.; Degtyarev, K.E.; Cuthbert, S.J.; Batanova, V.G.; Kovalchuk, E.V. Eclogites and garnet clinopyroxenites in the Anrakhai complex, Central Asian Orogenic Belt, Southern Kazakhstan: P-T evolution, protoliths and some geodynamic implications. *J. Asian Earth Sci.* **2018**, *153*, 325–345. [CrossRef]
14. Zhang, C.; Bader, T.; Zhang, L.M.; Shen, T.T.; Li, P.; Li, X.-P. Metamorphic evolution and age constraints of the garnet-bearing mica schist from the Xindaduo area of the Sumdo (U) HP metamorphic belt, Tibet. *Geol. Mag.* **2019**, *156*, 1175–1189. [CrossRef]
15. Li, X.-P.; Chen, H.-K.; Wang, Z.-L.; Wang, L.-J.; Yang, J.-S.; Robinson, P. Textural evolution of spinel peridotite and olivine websterite in the Purang ophiolite complex, western Tibet. *J. Asian Earth Sci.* **2015**, *110*, 55–71. [CrossRef]
16. Ishikawa, A.; Maruyama, S.; Komiya, T. Layered lithospheric mantle beneath the Ontong Java Plateau: Implications from xenoliths in Alnoite, Malaita, SolomonIslands. *J. Petrol.* **2004**, *45*, 2011–2044. [CrossRef]

17. Xiong, F.; Meng, Y.; Yang, J.; Liu, Z.; Xu, X.; Eslami, A.; Zhang, R. Geochronology and petrogenesis of the mafic dykes from the Purang ophiolite: Implications for evolution of the western Yarlung-Tsangpo suture zone, Tibet. *Geosci. Front.* **2019**, *11*, 277–292. [CrossRef]
18. Zhang, R.Y.; Liou, J.G. Clinopyroxenite from the Sulu ultrahigh-pressure terrane, eastern China: Origin and evolution of garnet exsolution in clinopyroxene. *Am. Mineral.* **2003**, *88*, 1591–1600. [CrossRef]
19. Xu, Z.Q.; Zeng, L.S.; Liu, F.; Yang, J.S.; Zhang, Z.M.; McWilliams, M.; Liou, J.G. Polyphase subduction and exhumation of the Sulu high-pressure–ultrahigh-pressure metamorphic terrane. In *Ultrahigh-Pressure Metamorphism: Deep Continental Subduction*; Special Paper 403; Geological Society of America: Boulder, CO, USA, 2006; pp. 93–113. [CrossRef]
20. Wang, S.J.; Li, X.P.; Schertl, H.P.; Feng, Q.D. Petrogenesis of early cretaceous andesite dykes in the Sulu orogenic belt, eastern China. *Mineral. Petrol.* **2019**, *113*, 77–97. [CrossRef]
21. Liu, F.L.; Xu, Z.Q.; Yang, J.S.; Zhang, Z.M.; Xue, H.M.; Li, T.F. Geochemical characteristics and UHP metamorphism of granitic gneisses in the maindrilling hole of Chinese Continental Scientific Drilling Project and its adjacent area. *Acta Petrol. Sin.* **2004**, *20*, 9–26.
22. Hiramatsu, N.; Hirajima, T. Petrology of the Hujialin garnet clinopyroxenite in the Su-Lu ultrahigh-pressure province, eastern China. *Island Arc.* **1995**, *4*, 310–323. [CrossRef]
23. Chen, J.; Xu, Z. Pargasite and ilmenite exsolution texture in clinopyroxenes from the Hujialing garnet-pyroxenite, Su-lu UHP terrane, central China: A geodynamic implication. *Eur. J. Mineral.* **2005**, *17*, 895–903. [CrossRef]
24. Zhang, R.Y.; Zhai, S.M.; Fei, Y.W.; Liou, J.G. Titanium solubility in coexistinggarnet and clinopyroxene at very high pressure: The significance of exsolved rutile ingarnet. *Earth Planet. Sci. Lett.* **2003**, *216*, 591–601. [CrossRef]
25. Zhang, R.Y.; Liou, J.G.; Huberty, J.M.; Xu, H.; Maki, K.; Jahn, B.-M.; Iizuka, Y. Origin and Metamorphic Evolution of Garnet Clinopyroxenite from the Sulu UHP Terrane, China. *Ultrah. Press. Metamorph.* **2011**, 151–185. [CrossRef]
26. Yang, J.-J. Ca-rich garnet clinopyroxenite rocks at Hujialin in the SuLu terrane (eastern China): Deeply subducted arc cumulates? *J. Petrol.* **2006**, *47*, 965–990. [CrossRef]
27. Li, T.F.; Yang, J.S.; Zhang, R.Y. Geochemical Characteristics, UHP Metamorphic Age, and Genesis of the Hujialing Garnet Clinopyroxenite, Sulu Terrane, China. *Int. Geol. Rev.* **2008**, *50*, 48–60. [CrossRef]
28. Xie, Z.P.; Wang, J.; Hattori, K.; Xue, C.D.; Zhong, J.W.; Wang, Z.L. The petrogenesis and tectonic implication of Hujialin ultramafic rocks in the Sulu ultrahigh-pressure metamorphic belt, eastern China. *Acta Petrol. Sin.* **2018**, *34*, 1539–1556. (In Chinese)
29. Zhao, R.X.; Liou, J.G.; Tsujimori, T.; Zhang, R.Y. Petrology and U-Pb SHRIMP geochronology of a garnet peridotite, Sulu UHP terrane, east-central China. *Int. Geol. Rev.* **2007**, *49*, 732–752. [CrossRef]
30. Gao, T.S.; Chen, J.F.; Xie, Z. Petrology and Geochemistry of Ultramafic Rocks at Hujialin, Sulu Orogen. *Bull. Mineral. Petrol. Geochem.* **2015**, *34*, 601–618. (In Chinese)
31. Zong, K.Q.; Klemd, R.; Yuan, Y.; He, Z.Y.; Guo, J.L.; Shi, X.L.; Liu, Y.S.; Hu, Z.C.; Zhang, Z.M. The assembly of Rodinia: The correlation of early Neoproterozoic (ca. 900 Ma) high-grade metamorphism and continental arc formation in the southern Beishan Orogen, southern central Asian Orogenic Belt (CAOB). *Precambrian Res.* **2017**, *290*, 32–48. [CrossRef]
32. Liu, Y.S.; Hu, Z.C.; Gao, S.; Günther, D.; Xu, J.; Gao, C.G.; Chen, H.H. In situ analysis of major and trace elements of anhydrous minerals by LA-ICP-MS without applying an internal standard. *Chem. Geol.* **2008**, *257*, 34–43. [CrossRef]
33. Ludwig, K. User's manual for Isoplot 3.00: A geochronological toolkit for Microsoft Excel. *Berkeley Geochronol. Cent. Spec. Publ.* **2003**, *1*, 1–55.
34. Whitney, D.L.; Evans, B.W. Abbreviations for names of rock-forming minerals. *Am. Mineral.* **2010**, *95*, 185–187. [CrossRef]
35. Obata, M.; Morten, L. Transformation of spinel lherzolite to garnet lherzolite in ultramafic lenses of the Austridic Crystalline Complex, northern Italy. *J. Petrol.* **1987**, *28*, 599–623. [CrossRef]
36. Staudigel, H.; Schreyer, W. The upper thermal stability of clinochlore, Mg_5Al $(AlSi_3O_{10})$ $(OH)_8$, at 10–35 kb PH_2O. *Contrib. Mineral. Petrol.* **1977**, *61*, 187–198. [CrossRef]
37. Schmidt, M.W.; Poli, S. Experimentally based water budgets for dehydrating slabs and consequences for arc magma generation. *Earth Planet. Sci. Lett.* **1998**, *163*, 361–379. [CrossRef]

38. Ulmer, P.; Trommsdorff, V. Serpentine stability to mantledepths and subduction-related magmatism. *Science* **1995**, *268*, 858–861. [CrossRef]
39. Alison, P. Chlorite stability in mantle peridotite: The reaction clinochlore + enstatite = forsterite + pyrope + H_2O. *Contrib. Mineral. Petrol.* **2003**, *144*, 449–456.
40. Yang, J.-J. Titanian clinohumite–garnet–pyroxene rock from the Su-Lu UHP metamorphic terrane, China: Chemical evolutionand tectonic implications. *Lithos* **2003**, *70*, 359–379. [CrossRef]
41. Chen, Y.; Su, B.; Guo, S. The Dabie-Sulu orogenic peridotites: Progress and key issues. *Sci. China Earth Sci.* **2015**, *58*, 1679–1699. (In Chinese) [CrossRef]
42. Yang, T.N.; Zeng, L.S.; Liou, J.G. Mineral evolutionof a garnet-pyroxenite nodule within eclogite, easternSulu ultrahigh-pressure metamorphic terrane, East China. *J. Metamorph. Geol.* **2005**, *23*, 667–680. [CrossRef]
43. Zeng, L.S.; Yang, T.N. Rongcheng Ultra-Calcic Garnet Pyroxenite:Its Geochemistry, Origin and Implications for Pre-UHP Tectonics in the Sulu UHP Metamorphic Belt. *Earth Sci.* **2006**, *31*, 488–496. (In Chinese)
44. McDonough, W.F.; Sun, S.S. The compositionof the Earth. *Chem. Geol.* **1995**, *120*, 223–254. [CrossRef]
45. Geng, Y.S.; Kuang, H.W.; Du, L.L.; Liu, Y.Q.; Zhao, T.P. On the Paleo-Mesoproterozoic boundary from the breakup event of the Columbia supercontinent. *Acta Petrol. Sin.* **2019**, *35*, 2299–2324.
46. Zheng, Y.F.; Wu, Y.B.; Zhao, Z.F.; Zhang, S.B.; Xu, P.; Wu, F.Y. Metamorphic effect on zircon Lu–Hf and U–Pb isotope systems in ultrahigh-pressure eclogite-facies metagranite and metabasite. *Earth Planet. Sci. Lett.* **2005**, *240*, 378–400. [CrossRef]
47. Wang, S.J.; Schertl, H.P.; Pang, Y.M. Geochemistry, geochronology and Sr-Nd-Hf Isotopes of two types of Early Cretaceous granite porphyry dykes in the Sulu Orogenic Belt, Eastern China. *Can. J. Earth Sci.* **2020**, *57*, 249–266. [CrossRef]
48. Zheng, Y.F. Fluid regime in continental subduction zones: Petrological insights from ultrahigh-pressure metamorphic rocks. *J. Geol. Soc.* **2009**, *166*, 763–782. [CrossRef]
49. Yang, J.S.; Wooden, J.L.; Wu, C.L.; Liu, F.L.; Xu, Z.Q.; Shi, R.D.; Katayama, I.; Liou, J.G.; Maruyama, S. SHRIMP U-Pb dating of coesite-bearing zircon from the ultrahigh-pressure metamorphic rocks, Sulu terrane, east China. *J. Metamorph. Geol.* **2003**, *21*, 551–560. [CrossRef]
50. Connolly, J.A.D. Multivariable phase-diagrams: An algorithm based on generalized thermodynamics. *Am. J. Sci.* **1990**, *290*, 666–718. [CrossRef]
51. Connolly, J.A.D. Computation of phase equilibria by linear programming: A toolfor geodynamic modeling and its application to subduction zone decarbonation. *Earth Planet. Sci. Lett.* **2005**, *236*, 524–541. [CrossRef]
52. Holland, T.J.B.; Powell, R. An internally consistent thermodynamic data set for phases of petrological interest. *J. Metamorph. Geol.* **1998**, *16*, 309–343. [CrossRef]
53. White, R.W.; Powell, R.; Holland, T.J.B.; Worley, B.A. The effect of TiO_2 and Fe_2O_3 on metapelitic assemblages at greenschist and amphibolite facies conditions: Mineralequilibria calculations in the system K_2O-FeO-MgO-Al_2O_3- SiO_2-H_2O-TiO_2-Fe_2O_3. *J. Metamorph. Geol.* **2000**, *18*, 497–511. [CrossRef]
54. Holland, T.; Powell, R. Thermodynamics of order-disorder in minerals: II. Symmetric formalism applied to solid solutions. *Am. Mineral.* **1996**, *81*, 1425–1437. [CrossRef]
55. Dale, J.; Holland, T.; Powell, R. Hornblende-garnet-plagioclase thermobarometry: A natural assemblage calibration of the thermodynamics of hornblende. *Contrib. Mineral. Petrol.* **2000**, *140*, 353–362. [CrossRef]
56. White, R.W.; Powell, R.; Clarke, G.L. The interpretation of reaction textures in Fe-rich metapelitic granulites ofthe Musgrave Block, central Australia: Constraints from mineral equilibria calculations in the system K_2O-FeO-MgO- Al_2O_3-SiO_2-H_2O-TiO_2-Fe_2O_3. *J. Metamorph. Geol.* **2002**, *20*, 41–55. [CrossRef]
57. Krogh Ravna, E.J. The garnet–clinopyroxene Fe^{2+}–Mg geothermometer: An updated calibration. *J. Metamorph. Geol.* **2000**, *18*, 211–219. [CrossRef]
58. Wang, S.J.; Wang, L.; Brown, M.; Feng, P.P. Multi-stage barite crystallization in partially melted UHP eclogite from the Sulu belt, China. *Am. Mineral.* **2016**, *101*, 564–579. [CrossRef]
59. Wang, L.; Kusky, T.M.; Polat, A.; Wang, S.J.; Jiang, X.; Zong, K.; Wang, J.P.; Deng, H.; Fu, J. Partial melting of deeply subducted eclogite from the Sulu orogen in China. *Nat. Commun.* **2014**, *5*, 5604. [CrossRef]
60. Schmidt, M.W. Amphibole composition in tonalite as a function of pressure: An experimental calibration of the Al-in-hornblende barometer. *Contrib. Mineral. Petrol.* **1992**, *110*, 304–310. [CrossRef]
61. Jahn, B.M. Geochemical and Isotopic Characteristics of UHP Eclogites and Ultramafic Rocks of the Dabie Orogen: Implications for Continental Subduction and Collisional Tectonics. *Petrol. Struct. Geol.* **1998**, *10*, 203–239.

62. Gonzaga, R.G.; Lowry, D.; Jacob, D.E.; LeRoex, A.; Schulze, D.; Menzies, M.A. Eclogites and garnet pyroxenites: Similarities and differences. *J. Volcanol. Geotherm. Res.* **2010**, *190*, 235–247. [CrossRef]
63. Zhang, X.; Li, X.P.; Wang, Z.L.; Zhao, L.Q.; Shi, T.Q.; Duan, W.Y. Mineralogical and Petrogeochemical characteristics of the garnet amphibolites in the Xigaze ophiolite, Tibet. *Acta Petrol. Sin.* **2016**, *32*, 3685–3702.
64. McCulloch, M.T.; Gamble, J.A. Geochemical and geodynamical constraints on subduction zone magmatism. *Earth Planet. Sci. Lett.* **1991**, *102*, 358–374. [CrossRef]
65. Davidson, J.P. Deciphering mantle and crustal signatures in subduction zone magmatism. *Geophys. Monogr.* **1996**, *96*, 251–264.
66. Wang, X.; Li, X.-P.; Han, Z.Z. Zircon ages and geochemistry of amphibolitic rocks from the Paleoproterozoic Erdaowa Group in the Khondalite Belt, North China Craton and their tectonic implications. *Precambrian Res.* **2018**, *317*, 253–267. [CrossRef]
67. Wang, X.; Li, X.-P.; Zhang, J.; Schertl, H.-P. Geochemistry, geochronology and evolution of Paleoproterozoic granitoid gneisses in the Khondalite Belt, North China Craton. *Precambrian Res.* **2020**, *338*. [CrossRef]
68. Zanetti, A.; Mazzucchelli, M.; Rivalenti, G.; Vannucci, R. TheFinero phlogopite-peridotite massif: An example of subductionrelated metasomatism. *Contrib. Mineral. Petrol.* **1999**, *134*, 107–122. [CrossRef]
69. Brueckner, H.K.; Medaris, L.G. A general model for the intrusion and evolution of mantle garnet peridotites in high-pressure and ultra-high-pressure metamorphic terranes. *J. Metamorph. Geol.* **2000**, *18*, 123–133. [CrossRef]
70. Li, X.-P.; Yang, J.-S.; Robinson, P.; Xu, Z.-Q.; Li, T.-F. Petrology and geochemistry of UHP-metamorphosed ultramafic–mafic rocks from the main hole of the Chinese Continental Scientific Drilling Project (CCSD-MH), China: Fluid/melt-rock interaction Mafic–ultramafic complex. *J. Asian Earth Sci.* **2011**, *42*, 661–683. [CrossRef]
71. Paquin, J.; Altherr, R. Subduction-related lithium metasomatism during exhumation of the Alpe Arami ultrahigh-pressuregarnet peridotite (Central Alps, Switzerland). *Contrib. Mineral. Petrol.* **2002**, *143*, 623–640. [CrossRef]
72. Li, X.-P.; Schertl, H.-P.; Reinhardt, J. Preface: Metamorphism and Orogenic Belts: Response from micro- to macro-scale. *J. Earth Sci.* **2019**, *30*, 1075–1083. [CrossRef]
73. Sun, G.; Li, X.-P.; Dun, W.; Chen, S.; Wang, Z.; Zhao, L.; Fen, Q. Metamorphic Characteristics and Tectonic Implications of the Kadui Blueschist in the Central Yarlung Zangbo Suture Zone, Southern Tibet. *J. Earth Sci.* **2018**, *29*, 1026–1039. [CrossRef]
74. Zhang, Y.-C.; Li, X.-P.; Sun, G.-M.; Wang, Z.-L.; Duan, W.-Y. Metamorphic petrology of clinopyroxene amphibolite from the Xigaze ophiolite, Southern Tibet: P-T constraints and phase equilibrium modeling. *J. Earth Sci.* **2019**, *30*, 549–562. [CrossRef]
75. Kong, F.-M.; Liu, Y.; Li, X.-P.; Guo, J.H.; Zhao, G.C. Mineralogical and Petrogeochemical characteristics of ultramafic rocks from the metamorphic basement of the Jiaobei terrane. *Acta Petrol. Sin.* **2015**, *31*, 1549–1563.
76. Groves, D.I.; Santosh, M. The giant Jiaodong gold province: The key to a unified model for orogenic gold deposits? *Geosci. Front.* **2016**, *7*, 409–417. [CrossRef]